Quasi-Resonant Vibration−Rotation Transfer in Inelastic Li_2*−Ne Collisions†

Brian Stewart*

Department of Physics, Wesleyan University, Middletown, Connecticut 06549

Peter D. Magill

Lucent Technologies, Murray Hill, New Jersey 07974

David E. Pritchard

Department of Physics and Research Laboratory of Electronics, Massachusetts Institute of Technology, Cambridge, Massachusetts 02139

Received: April 17, 2000; In Final Form: August 15, 2000

We present the results of a detailed study of the influence of rotational angular momentum on vibrotational transfer in the system $Li_2^*(v_i,j_i) + Ne \rightarrow Li_2^*(v_f,j_f) + Ne$, where $v_{i,f}$ and $j_{i,f}$ indicate initial and final vibrational and rotational levels, respectively, and Li_2* is in its first electronically excited $^1\Sigma_u^+$ state. Level-to-level inelastic rate constants for j_i up to 76 have been measured. The measurements span 4 orders of magnitude in size and include $|\Delta v| \leq 5$ and $|\Delta j| \leq 50$. The results extend the range of previous measurements in this system and further document the phenomenon of quasiresonant vibrotational transfer. This process, induced by high rotational angular momentum, results in large rate constants for vibrational transfer and a systematic correlation of Δj and Δv according to the rule $\Delta j = -4\Delta v$. At $j_i \geq 64$, the total vibrationally inelastic rate constant is found to be larger than the total rotationally inelastic rate constant. A fully classical treatment of the dynamics on an ab initio potential surface results in rate constants that agree remarkably well with the data.

I. Introduction

Inelastic atom−diatom transfer under ordinary conditions is dominated by rotational transfer; the probability of vibrationally inelastic transfer is generally orders of magnitude smaller. This is because, for most collisions at thermal velocities, the atom-molecule force contains only a small component at the oscillator frequency and the collisions are vibrationally adiabatic. For this reason, increased collision energy generally enhances vibrationally inelastic transfer.[1] However, molecules with small moments of inertia can have, at large j, rotational frequencies and energy level spacings comparable to those of the vibration. In such cases, the vibrational and rotational motions can become strongly coupled by the collision, and the probability of collisionally induced vibrational transfer can be greatly enhanced. In fact, rotational enhancement of vibrational transfer was proposed as early as 1962 by Cottrell and Matheson[2,3] to account for the observation that pure methane undergoes vibrational relaxation more rapidly than tetradeuteromethane. These authors reasoned that the larger average angular velocity of methane at a given temperature results in a greater effective collision velocity and, hence, an enhanced probability for vibrationally inelastic collisions.

Work at M. I. T. has resulted in the first level-resolved measurements of vibrational transfer at sufficiently high j_i to observe the onset of resonant vibration−rotation transfer. We present here a detailed experimental study of vibrotational transfer in the system $Li_2^*(v_i,j_i) + Ne \rightarrow Li_2^*(v_f, j_f) + Ne$, where $^7Li_2$* is in its first electronically excited $^1\Sigma_u^+$ state, v and j are its vibrational and rotational quantum numbers, and i and f refer to its initial and final quantum levels. This study extends the scope of previous experimental studies[4−6] of the effect of j_i on the vibrotationally inelastic transfer process and permits us to fully document the phenomenon known as quasiresonant vibrotational transfer that occurs at high j_i in Li_2 collisions. These level-to-level measurements span a large dynamic range and are unprecedented in the range of final quantum levels resolved. A short account of this work has appeared previously;[7] in this report we give full details of our many high-j inelastic rate constant measurements. Renewed interest in the phenomenon,[8−10] particularly at the extremely low temperatures now attainable in magneto-optic traps,[9] prompts us to give a detailed account of our data at this time. In addition, we present results of classical trajectory calculations on an ab initio potential surface that was not available at the time of our initial report.

The remainder of this section summarizes the hallmarks of the quasiresonant transfer process and reviews previous calculations and experiments that are relevant. Section II provides a brief description of the experiment and a summary of the technique we use to obtain level-to-level rate constants from collision spectra. Section III presents the rate constants and a description of their main features. Section IV contains results of classical trajectory calculations on an ab initio potential surface that agree remarkably well with the data, as well as a discussion of some of the issues that arise when binning quasiclassical trajectories for a process that is sharply peaked with respect to the final action. Section V is devoted to a brief discussion of the mechanism of quasiresonant transfer and a review of recent relevant literature.

A. Quasiresonant Vibrotational Transfer. The first level-to-level rate constant measurements in the similar system Li_2*−Xe were made by Saenger et al.[4] They found that increased

† Part of the special issue "C. Bradley Moore Festschrift".

* Corresponding author. E-mail: bstewart@wesleyan.edu.

10.1021/jp001445c CCC: $19.00
Published on Web 10/25/2000

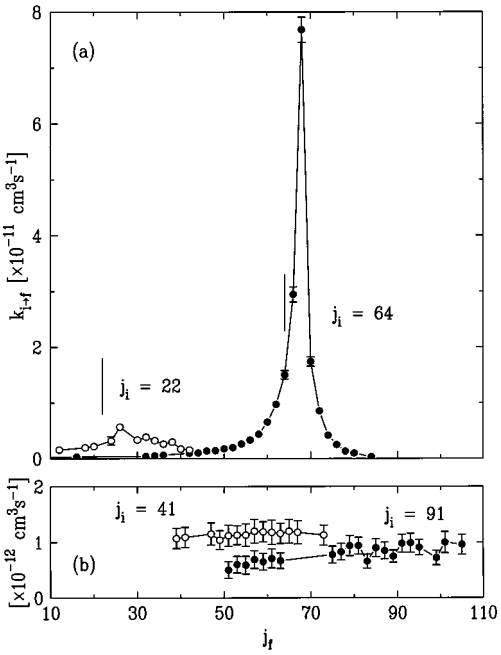

Figure 1. (a) Experimental level-to-level rate constants for Li_2*−Ne with $j_i = 22$ and 64 and $\Delta v = -1$ demonstrate the striking enhancement of vibrotational transfer and systematic shift of the j_f-distribution at high rotational angular momentum. Vertical lines indicate j_i. The data for $j_i = 22$ are from ref 12. (b) The I_2*−Xe system shows none of these features, even at $j_i = 91$. Data are from ref 14. The ordinate scales differ by an order of magnitude in the two figures.

rotation enhances the rate constant for vibrotational transfer and results at $j_i = 44$, in a large negative correlation of Δj and Δv. Subsequent work[7,11,12,6] has resulted in a more complete characterization of this phenomenon:

1. The vibrotationally inelastic rate constant rises as j_i increases and becomes sharply peaked at a specific j_f.

2. Δv and Δj are highly correlated at the peak of the j_f distributions according to the rule $\Delta j^{peak} = -4\Delta v$.

3. Cross section measurements made using the Doppler VSDS technique[6,7] show that peaking of the rate constant distribution is enhanced at low collision velocity.

4. The process is quite insensitive to the detailed nature of the interaction potential;[11,13] in particular, the presence or absence of a substantial potential well has little effect.

5. At large j_i, vibrationally inelastic collisions are more probable than purely rotationally inelastic collisions.

The sharp peaking of the j_f distribution for each Δv and the systematic shift of this peak with Δv implicate vibration−rotation resonance as the mechanism for this process, but the empirical rule $\Delta j^{peak} = -4\Delta v$ does not always result in complete intramolecular energy conservation, which is given, for example, by $\Delta j = -6\Delta v$ at $j_i = 44$. For this reason, we have termed the process quasiresonant vibrotational transfer (QVRT).

In the present study, we have extended the range of j_i and applied improved data collection and analysis techniques to extend the range of Δj and Δv as well. The result is rate constant distributions for $44 \le j_i \le 76$ spanning 4 orders of magnitude in size. The measurements include $|\Delta v|$ as large as 5 and $|\Delta j|$ as large as 50. The largest of the vibrotationally inelastic rate constants, $k_{v_i=5,j_i=64\to 4,68}$, corresponds to a thermally averaged level-to-level cross section of nearly 8 Å^2 and is nearly equal in size to the largest rotationally inelastic rate constant for the same j_i. Figure 1a shows experimental results for $j_i = 22$ and 64 with $\Delta v = -1$, illustrating the enhancement of the vibrationally inelastic rate constant, the systematic shift of Δj with Δv, and the narrowing of the j_f distribution at large j_i. For comparison, results for I_2*−Xe collisions[14] are shown in Figure 1b. The I_2*−Xe system, with its much smaller rotational frequency and energy level spacing for a given j, exhibits none of the features of quasiresonant vibrotational transfer.

TABLE 1: Features of QVRT Seen in Previous Calculations

system	enhancement at high j_i	systematic shift of peak	enhancement at low v_{rel}	type of calculation[a]	ref
H_2−He		X		EP	15
	X	X		EP	16
	X	X		SC	17,18
		X		CS	19
	X	X	X	QCT	20
	X	X		QCT	21
	X	X		CC	22
H_2−Ar	X			SC	23
	X	X		QCT	24
HF−He, Ne		X		QCT	25
HF−Ar	X	X	X	QCT	26
HCl−Ar	X	X		QCT	27

[a] Key to abbreviations: EP, effective potential calculation; SC semiclassical; CS, coupled states; QCT, quasiclassical trajectories; CC, close coupled.

B. Signs of Resonance in Previous Calculations and Experiments. Early calculations that showed some of the features of quasiresonant vibrotational transfer outlined above are summarized in Table 1. It is noteworthy that the molecules included in Table 1 all have small moments of inertia and hence large rotational energy spacings and large rotational frequencies for a given j_i. Energy spacings comparable to the vibrational energy spacing are a necessary condition for resonance, for they make it possible for the final molecular level to have nearly the same energy as the initial level after a vibrationally inelastic collision without necessitating a large change in the molecular angular momentum. The particularly exhaustive quasiclassical study of Dove et al.[20] for H_2−He varied j_i from 0 to 34[28] and E_{rel} from 3 to 100 kcal mol^{-1}, and presented contour diagrams of the rate constant distributions that show the dramatic negative correlation of Δv and Δj that develops in this system for $j_i \ge 16$. The H_2−He calculations of Dove and others found Δv and Δj to be correlated according to the rule $\Delta j^{peak} = -2\Delta v$, independent of j_i; the quantal calculations listed in Table 1 found this rule to hold for j_i as low as 4. This condition leaves the molecular term energy nearly unchanged for large j_i (≥ 12), but for $j_i = 10$, energy resonance requires $\Delta j/\Delta v = -4$, and for $j_i = 8$ the ratio would be −6 or −8. This is completely analogous to the QVRT phenomenon observed in Li_2*−Ne: the most probable $|\Delta j/\Delta v|$ does not exceed 4 in this system, even though exact internal energy conservation would require it to do so. In a perceptive semiclassical study entitled "The Influence of Molecular Rotation on Vibration-Translation Energy Transfer",[18] McKenzie pointed out that, because of limitations on angular momentum transfer, "vibration−rotation transitions with small Δj will dominate the intermolecular energy transfer process, regardless of resonance."

Few absolute level-to-level measurements of vibrotational transfer at elevated j_i have been made in systems other than Li_2*−X (where X is a noble gas). To our knowledge, only I_2*−X has been studied in any detail.[29,14] Dexheimer et al.[14] measured rate constants with j_i equal to 41 and 91 and found essentially no difference between the resulting j_f distributions and none of the features of QVRT enumerated in section IA (see Figure 1b).

TABLE 2: Synopsis of Experimental Measurements of Level-Resolved Vibrotational Transfer in Li_2 $A^1\Sigma_u^+$−Ne[a]

j_i	v_i	Δv range	Δj range	T_{oven} (K)	T_{eff} (K)	n_{Li} (cm^{-3})	n_{Li2} (cm^{-3})	$\bar{v}_{rel}$ (km/s)	ref
8	9	−3 to 0	−6 to 42	868	697	5.0×10^{14}	6.7×10^{12}	1.34	12
22	9	−3 to 0	−20 to 28	863	693	4.4×10^{14}	5.7×10^{12}	1.33	12
30	2−24	−2 to 2	−30 to 46	898	721	9.8×10^{14}	1.6×10^{13}	1.36	48
44	4	−3 to 4	−44 to 36	880	707	6.6×10^{14}	9.5×10^{12}	1.35	this work
50	4	−3 to 4	−50 to 32	892	717	8.6×10^{14}	1.3×10^{13}	1.36	this work
64	5	−4 to 4	−58 to 24	891	716	8.4×10^{14}	1.3×10^{13}	1.35	this work
76	7	−5 to 3	−38 to 14	922	740	1.6×10^{15}	3.0×10^{13}	1.38	this work

[a] Lithium atomic and molecular densities are from the data of ref 45.

Vibrational transfer in the Li_2*−X system was explored previously by Ennen and Ottinger[30] in the $B^1\Pi_u$ electronic state. These authors found a systematic shift of the peak in the j_f distributions in collisions with Ar with Δv ranging from −4 to +2. They did not vary j_i systematically, however, and the limited resolution of their experiment did not permit them to quantify the observed shift with Δv. Vibrotational transfer at high j_i in the Li_2*$A^1\Sigma_u^+$ electronic state has been the subject of several previous studies in this laboratory.[4−6,11,12] In the present work, we have extended these experimental studies up to $j_i = 76$ in Li_2*−Ne, observing for the first time a true energy resonance at $j_i = 64$.

Finally, it is worth noting that rotational enhancement of vibrational transfer has been observed in polyatomic systems. The original observations of rotational enhancement in CH_4 by Cottrell and Matheson[2] were confirmed by Zittel and Moore[31] and more recently by Perrin and Jolicard.[32] Moore has also discussed *inter*molecular vibration−rotation transfer.[33] Cottrell et al.[34] also inferred vibration−rotation transfer in AsH_3.

II. Experimental Section

The experimental technique is a standard one that has been employed by ourselves and others repeatedly. We outline it briefly here, indicating in detail where our procedures differ from those used previously.

A. Experimental Design and Data Acquisition. The experiment is based on a laser-induced fluorescence technique used extensively at M. I. T. and elsewhere to measure rate constants for alkali dimer−rare gas scattering. The most important feature of the experiment is that collisions occur in an electronically excited state. The ca. 18 ns natural lifetime of the Li_2 $A^1\Sigma_u^+$ state makes single collision conditions accessible in a cell at rare gas pressures on the order of 1 Torr.

In our experiment, a particular initial level (v_i,j_i) is selected in the $A^1\Sigma_u^+$ state by means of a single-mode continuous-wave dye laser. At low target gas pressure, the fluorescence spectrum emanating from this level consists of a series of PR doublets, which are termed *parent lines*. As the target gas pressure is increased, collisional transfer within the excited state from (v_i,j_i) to (v_f,j_f) becomes important, and a new series of spectral lines becomes observable. These *satellite lines* originate from excited-state levels that are populated by collisions of Li_2* molecules with rare gas atoms. It is the intensities of these lines, after normalization by transition strength and parent line intensity, that yield the inelastic rate constants. The fluorescence spectrum is obtained by focusing the emission from a cell containing hot laser-excited lithium and neon gas onto the entrance slit of a double monochromator. Photon counting is employed, and magic angle detection is used to minimize alignment effects.[35] The spectrum is recorded for several target gas pressures. The rate constants are then recovered from fits to the pressure dependence of the normalized satellite line intensities. Details of the experimental setup and data acquisition procedure are as given in ref 36.

B. Analysis of the Data. We outline here the produres involved in obtaining rate constants from the spectral data. Complete details have been given previously.[12,36,37] The spectra are first corrected for laser power fluctuations; we estimate the residual uncertainty in the measurements due to laser power fluctuation to be ≤5%. The spectral lines are then assigned. Semiautomatic assignment of the spectra is possible because the spectroscopy of the Li_2 A−X transition is well-known.[38−40] A correction is made for pulse pileup errors, and the spectral background (typically several tens of counts per second) is subtracted. The highest three points on each spectral line are added and used as a measure of the intensity.

After a correction is applied for instrument response, the intensities are normalized by transition strength. We have found that it is insufficiently accurate to use *j*-dependent Franck−Condon factors, since the Li_2 A−X electronic transition moment has a substantial dependence on internuclear separation.[41] We therefore calculate vibrational bandstrengths using the RKR potentials of Kusch and Hessel[38] and the *r*-dependent transition moment of Schmidt-Mink et al.[41] The resulting bandstrengths can exhibit a variation of 25% as *j* varies from 0 to 80, even for a strong transition.

The excited-state population density in a final level *f* may be modeled as

$$\frac{dn_f}{dt} = k_{if} n_i n_X + k_{if}^{Li} n_i n_{Li} - k_Q n_f n_X - k_Q^{Li} n_f n_{Li} - \Gamma_f n_f \quad (1)$$

Here k_{if} is the desired inelastic rate constant, n_i and n_X are the densities of the initially populated level and the rare gas, respectively, k_{if}^{Li} is the rate constant for inelastic population of the final level f through lithium atom collisions, k_Q and k_Q^{Li} represent depopulation of the final level f through inelastic and quenching collisions with the rare gas and atomic lithium, respectively, and Γ_f is the radiative decay rate of the final state. Solution of this equation in steady-state yields the expression

$$\frac{n_f}{n_i} = \frac{k_{if}^{Li} n_{Li} + k_{if} n_X}{\Gamma_f + k_Q^{Li} n_{Li} + k_Q n_X} \quad (2)$$

Ratios of corrected and normalized intensities are employed as measures of the population ratios; least-squares fits of eq 2 to our pressure-dependent data yield the rate constant. The radiative lifetime $1/\Gamma_f$ varies from about 18 to 19 ns over the range of molecular term energies accessed in our experiment; we model this variation using the lifetime data of Baumgartner et al.[42,43] Because $k_Q^{Li} n_{Li}$ is a constant for a given final level, this term combines with Γ_f to produce an effective decay rate that is larger than the natural decay rate. The rate constant determined from eq 2 by varying the rare gas pressure thus underestimates the true rate constant. Using the quenching cross section $\sigma_Q^{Li} = 150 \pm 50$ Å^2 reported by Derouard and Sadeghi[44] and lithium densities and mean collision speeds from Table 2, we estimate that the rate constants we report for $j_i = 44$ are low by

TABLE 3: Measured Inelastic Rate Constants for Li_2 $A^1\Sigma_u^+$−Ne Collisions with $j_i = 44$ and $v_i = 4$[a]

j_f	−3	−2	−1	0	1	2	3	4
0				0.032(0.006)				
2			0.011(0.004)	0.097(0.013)	0.014(0.003)			
4				0.208(0.025)	0.016(0.004)	0.005(0.002)		
6	0.001(0.002)		0.028(0.006)	0.277(0.025)	0.025(0.005)	0.005(0.002		
8		0.008(0.002)		0.323(0.010)	0.029(0.006)	0.008(0.002)		
10		0.012(0.003)	0.038(0.007)	0.480(0.023)	0.036(0.004)	0.014(0.005)		
12	0.005(0.002)		0.051(0.008)	0.488(0.045)	0.054(0.008)	0.017(0.004)		
14		0.019(0.004)	0.055(0.009)	0.581(0.016)	0.065(0.004)	0.014(0.004)		
16	0.006(0.002)	0.013(0.003)	0.066(0.003)	0.677(0.007)	0.090(0.013)	0.020(0.004)		
18		0.021(0.005)	0.071(0.010)	0.841(0.075)	0.096(0.007)	0.017(0.004)		
20	0.011(0.003)		0.084(0.011)	1.006(0.158)	0.100(0.013)	0.026(0.005)	0.013(0.004)	
22		0.043(0.009)	0.108(0.013)	1.003(0.327)	0.148(0.016)			
24		0.043(0.008)	0.112(0.014)	1.109(0.055)	0.123(0.006)	0.039(0.007)	0.010(0.003)	
26	0.011(0.006)	0.036(0.003)	0.129(0.006)	1.246(0.137)	0.171(0.019)	0.050(0.010)	0.014(0.004)	
28	0.038(0.007)	0.060(0.009)	0.160(0.019)	1.580(0.065)	0.205(0.025)	0.058(0.009)	0.021(0.005)	
30	0.027(0.003)	0.043(0.008)	0.175(0.019)	1.776(0.049)	0.245(0.028)	0.086(0.016)	0.019(0.004)	0.006(0.002)
32	0.028(0.006)		0.189(0.003)	2.383(0.102)	0.328(0.023)	0.106(0.018)	0.023(0.005)	0.009(0.003)
34	0.022(0.005)	0.055(0.009)	0.222(0.021)	2.896(0.117)	0.442(0.054)	0.105(0.014)	0.026(0.005)	
36	0.033(0.006)	0.068(0.010)	0.262(0.000)	3.888(0.054)	0.530(0.011)	0.126(0.037)	0.029(0.002)	0.009(0.003)
38	0.071(0.018)	0.093(0.013)	0.378(0.035)	5.271(0.178)	1.204(0.491)	0.148(0.031)	0.020(0.001)	
40	0.064(0.010)	0.067(0.011)	0.433(0.015)	8.230(0.316)	1.251(0.034)	0.100(0.014)		
42	0.039(0.007)	0.097(0.018)	0.585(0.011)	16.560(1.579)	0.831(0.039)	0.084(0.000)	0.022(0.005)	0.015(0.004)
44	0.040(0.007)	0.139(0.018)	0.816(0.015)		0.597(0.033)	0.072(0.010)		
46	0.043(0.007)	0.135(0.014)	1.209(0.020)	14.460(0.340)	0.439(0.062)	0.061(0.010)	0.005(0.003)	
48	0.055(0.008)	0.138(0.016)	2.335(0.132)	5.823(0.176)	0.259(0.027)	0.039(0.007)	0.013(0.005)	
50		0.235(0.022)	1.142(0.054)	3.306(0.147)	0.253(0.014)	0.039(0.009)	0.012(0.003)	0.003(0.001)
52	0.052(0.002)	0.310(0.026)	0.680(0.058)	1.538(0.041)	0.140(0.024)	0.024(0.005)	0.014(0.007)	
54	0.045(0.009)	0.249(0.025)	0.490(0.031)	0.990(0.064)	0.090(0.012)	0.020(0.006)	0.003(0.002)	0.003(0.001)
56	0.076(0.012)	0.210(0.021)	0.306(0.027)	0.587(0.081)	0.069(0.010)	0.009(0.003)		
58	0.036(0.006)	0.106(0.014)	0.196(0.026)	0.452(0.034)	0.070(0.010)	0.012(0.004)		
60	0.045(0.009)	0.085(0.012)		0.236(0.024)	0.040(0.010)			
62		0.069(0.010)	0.073(0.010)	0.185(0.019)	0.026(0.008)			
64	0.027(0.006)	0.029(0.006)	0.081(0.011)	0.108(0.013)	0.017(0.004)			
66		0.026(0.005)	0.063(0.015)	0.074(0.010)	0.016(0.004)			
68	0.017(0.005)	0.025(0.005)	0.052(0.008)	0.058(0.009)				
70			0.034(0.006)					
72		0.019(0.005)			0.002(0.005)			
74	0.003(0.002)		0.021(0.005)					
76								
78								
80					0.001(0.001)			

[a] In units of 10^{-11}cm^3 s^{-1}. The error estimates, given in parentheses in the same units, include statistical errors accumulated during the analysis.

approximately 2% due to the neglect of this term. The error rises to about 3% for $j_i = 50$ and 64 and to almost 6% for $j_i = 76$, for which signal requirements necessitated a hotter cell with a larger n_{Li2} but also a larger n_{Li}. Owing to the uncertainty in σ_Q^{Li}, we have elected to note the error but not correct for it in our reported measurements. However, in a few cases a molecular transition involving the final state f nearly coincided with the atomic lithium resonance transition, resulting in a substantial lifetime shortening due to resonant lithium atom quenching. Several excited-state levels required correction for this more dramatic lifetime shortening, for which we used the data of Baumgartner et al.[46]

Since we are able to record fluorescence on several different molecular bands, we often have multiple measures of a particular rate constant, and these are averaged together. We estimate that the largest of our measured rate constants are subject to uncertainties of 5−10%, while small rate constants, which often are determined from a single molecular line, have uncertainties in the vicinity of 30%. The reported uncertainties are often smaller, as they reflect only statistical error accumulated in the course of the analysis.

Because the laser is tuned to resonance, only molecules with no velocity component along the laser axis are excited. The distribution of collision speeds is therefore not a Maxwell−Boltzmann distribution at the temperature of the oven. However, it has been demonstrated[47] that the actual distribution of collision speeds in our experiment is well-approximated (especially in the case of the light neon target atom) by a Maxwell−Boltzmann distribution at a reduced temperature T_{eff}:

$$T_{eff} = T_{oven}\left(1 - \frac{1}{3(1+r)}\right) \qquad (3)$$

where r is the ratio of the laser excited diatom mass to that of the colliding atom. In our experiment, the ratio of effective to oven temperatures is 0.803. Oven and effective temperatures are given in Table 2, as are mean collision speeds and the densities of Li and Li_2.

III. Experimental Results

In this section we present the rate constants resulting from the analysis detailed in section II and draw attention to the main features that characterize them.

A. The Inelastic Rate Constants. We have measured 628 level-to-level rate constants for the process Li_2^* $A^1\Sigma_u^+$ (v_i,j_i) + Ne → $Li_2^*(v_f,j_f)$ + Ne at four different j_i. The values of j_i and v_i for which we present data, as well as collision energies and velocities, are given in Table 2, and the experimentally determined rate constants and their uncertainties are given in Tables 3−6. The data are displayed in Figures 2−5.

TABLE 4: Measured Inelastic Rate Constants for Li_2 $A^1\Sigma_u^+$−Ne Collisions with $j_i = 50$ and $v_i = 4$[a]

j_f	−3	−2	−1	0	1	2	3	4
0					0.014(0.003)			
2					0.050(0.008)			
4					0.104(0.013)			
6			0.022(0.005)	0.128(0.015)		0.003(0.001)		
8		0.010(0.003)		0.170(0.015)	0.023(0.006)	0.013(0.003)		
10		0.017(0.004)	0.032(0.006)	0.190(0.019)	0.031(0.006)	0.015(0.004)		
12	0.006(0.003)		0.039(0.007)					
14			0.037(0.014)	0.282(0.025)	0.063(0.009)	0.017(0.004)		
16	0.013(0.004)		0.053(0.008)	0.314(0.022)	0.066(0.011)	0.022(0.005)		
18		0.024(0.005)	0.067(0.010)	0.351(0.041)	0.087(0.011)			
20	0.013(0.005)		0.072(0.010)	0.437(0.113)	0.092(0.015)	0.034(0.006)		
22			0.067(0.010)	0.477(0.044)	0.087(0.012)			
24			0.087(0.012)	0.494(0.027)	0.095(0.016)	0.042(0.007)		
26	0.020(0.004)	0.036(0.007)	0.081(0.011)	0.597(0.046)	0.127(0.015)			
28	0.017(0.004)	0.040(0.007)	0.117(0.014)	0.705(0.076)	0.162(0.017)	0.056(0.010)		
30	0.025(0.005)	0.044(0.009)	0.123(0.014)	0.836(0.060)	0.173(0.018)		0.021(0.005)	
32	0.023(0.005)		0.135(0.015)	0.980(0.065)	0.195(0.018)			
34	0.034(0.007)	0.045(0.009)	0.157(0.017)	1.183(0.064)	0.255(0.023)	0.077(0.011)	0.025(0.005)	
36		0.049(0.008)	0.177(0.019)	1.419(0.072)	0.303(0.026)	0.120(0.015)	0.032(0.006)	
38				1.814(0.085)	0.491(0.082)	0.205(0.041)	0.032(0.006)	
40		0.058(0.009)	0.247(0.023)	2.279(0.018)	0.523(0.045)	0.212(0.023)		
42		0.073(0.011)	0.308(0.026)	3.049(0.048)	0.633(0.082)	0.227(0.022)	0.034(0.006)	
44	0.025(0.006)	0.075(0.011)	0.397(0.031)	4.141(0.255)	1.227(0.073)	0.222(0.021)		
46	0.041(0.009)	0.102(0.013)	0.506(0.037)	7.333(0.410)	2.621(0.116)	0.160(0.017)		
48		0.112(0.014)	0.735(0.047)	14.900(0.244)	1.155(0.122)	0.078(0.011)		
50		0.142(0.016)	1.042(0.059)		0.776(0.068)		0.012(0.003)	0.009(0.003)
52	0.051(0.009)	0.205(0.020)	1.716(0.082)	12.250(0.873)	0.446(0.009)	0.054(0.009)		
54	0.028(0.006)	0.223(0.022)	4.263(0.149)	4.689(0.050)	0.323(0.032)	0.043(0.009)	0.008(0.003)	
56		0.423(0.033)	1.577(0.078)	2.272(0.218)	0.190(0.020)		0.002(0.002)	
58	0.057(0.013)	0.562(0.039)	0.814(0.050)	1.284(0.059)	0.154(0.017)	0.028(0.006)		
60		0.379(0.030)	0.705(0.046)	0.768(0.050)				
62		0.184(0.019)	0.313(0.027)	0.415(0.032)	0.075(0.005)			
64		0.125(0.017)		0.276(0.025)	0.049(0.016)			
66		0.085(0.011)	0.140(0.016)	0.175(0.018)	0.036(0.000)	0.011(0.003)		
68		0.060(0.009)	0.111(0.013)	0.098(0.012)				
70			0.070(0.010)	0.087(0.012)				
72		0.038(0.007)			0.021(0.004)			
74			0.036(0.007)					
76								
78								
80			0.020(0.005)		0.004(0.002)			
82					0.004(0.002)			

[a] In units of 10^{-11}cm^3 s^{-1}. The error estimates, given in parentheses in the same units, include statistical errors accumulated during the analysis.

The most striking feature of our data at elevated j_i is the development of the QVRT phenomenon.[7] Scrutiny of Figures 2−5 reveals the dramatic increase in the vibrationally inelastic rate constant with rising j_i and the narrowing of the distribution of j_f values; these are the hallmarks of QVRT.

An equally characteristic feature of QVRT is the systematic shift of the peak in the j_f distribution with Δv. For $j_i = 64$, the peak position obeys the rule

$$\Delta j^{peak} = -4\Delta v \tag{4}$$

for $-3 \le \Delta v \le 3$. This rule holds very nearly for $-2 \le \Delta v \le 2$ for all other $j_i \ge 44$ as well. The importance of the linear correlation of Δj and Δv lies in the fact that it precludes exact intramolecular energy resonance as the sole mechanism of QVRT. Internal molecular energy is conserved when rotational and vibrational energy changes are equal and opposite, i.e.,

$$B_v[j_f(j_f + 1) - j_i(j_i + 1)] = -\omega_v(v_f - v_i) \tag{5}$$

At large j, this equation becomes equal to its classical analogue

$$2B_v j_i \Delta j^{peak} = -\omega_v \Delta v \tag{6}$$

This formula predicts a $\Delta j^{peak}/\Delta v$ ratio ranging from −6 at $j_i = 44$ to −3.4 at $j_i = 76$ and gives the observed ratio $\Delta j^{peak}/\Delta v = -4$ only for $j_i = 64$. It is this observation that suggested the term quasiresonant to describe the process: the narrow peaks and negative correlation of Δj and Δv are reminiscent of internal energy resonance, but the fact that the ratio $\Delta j/\Delta v$ is independent of j_i indicates the importance of factors other than energy resonance.

B. j_f-Summed Rate Constants. The j_f-summed rate constants are tabulated in Table 7. Where necessary, reasonable interpolations and extrapolations were made to account for missing data. Such extrapolations are small, except for the largest values of $|\Delta v|$, and were made, where possible, using the distributions for neighboring Δv or for a different target gas[12] as a template. The uncertainties were calculated assuming a 100% uncertainty in the interpolated and extrapolated rate constants. A caveat is in order regarding the quantitative use of the data in Table 7. Since v_i could not be held constant for all the data, direct comparison of data with large Δv and differing v_i should be made with caution. The effect of v_i on the rate constants is discussed in greater detail in the next section.

Several points emerge from a consideration of the data of Table 7:

(1) The total rotationally inelastic rate constant ($\Delta v = 0$)

TABLE 5: Measured Inelastic Rate Constants for Li_2 $A^1\Sigma_u^+$−Ne Collisions with $j_i = 64$ and $v_i = 5$[a]

j_f	−4	−3	−2	−1	0	1	2	3	4
6				0.014(0.004)					
8									
10			0.012(0.003)						
12									
14			0.023(0.005)						
16			0.019(0.005)	0.031(0.006)					
18		0.010(0.003)	0.026(0.006)						
20			0.020(0.005)		0.074(0.011)				
22			0.027(0.011)		0.082(0.011)				
24					0.098(0.013)				
26			0.030(0.006)		0.117(0.012)				
28		0.018(0.012)			0.131(0.015)	0.070(0.011)			
30		0.011(0.003)	0.028(0.006)		0.192(0.030)				
32		0.015(0.004)		0.042(0.007)	0.182(0.019)	0.118(0.021)			
34		0.026(0.008)		0.053(0.010)	0.178(0.022)	0.103(0.016)			
36			0.046(0.010)	0.065(0.011)	0.184(0.019)	0.114(0.016)		0.041(0.014)	
38		0.033(0.006)			0.277(0.050)		0.060(0.009)		
40		0.035(0.006)	0.049(0.010)		0.288(0.10)	0.148(0.016)			
42	0.032(0.006)	0.029(0.006)	0.050(0.008)	0.096(0.013)	0.302(0.004)	0.204(0.017)			
44			0.041(0.013)	0.102(0.015)	0.325(0.011)	0.189(0.019)		0.070(0.012)	
46			0.050(0.009)	0.138(0.016)	0.424(0.016)	0.284(0.029)	0.119(0.021)	0.095(0.023)	
48		0.025(0.005)	0.066(0.011)	0.143(0.016)	0.421(0.035)	0.252(0.028)	0.243(0.023)		
50			0.063(0.009)	0.178(0.020)	0.609(0.024)	0.386(0.072)	0.256(0.023)	0.146(0.034)	0.051(0.008)
52			0.072(0.012)	0.198(0.022)	0.796(0.049)	0.499(0.035)	0.330(0.052)	0.334(0.028)	0.065(0.030)
54	0.029(0.006)		0.083(0.012)	0.263(0.025)	1.008(0.013)	0.748(0.051)	0.624(0.042)	0.223(0.023)	
56			0.133(0.017)	0.334(0.029)	1.472(0.007)	1.021(0.132)	1.349(0.071)		
58		0.046(0.007)	0.126(0.015)	0.437(0.034)	2.224(0.014)	1.863(0.117)	0.581(0.041)	0.091(0.068)	
60		0.059(0.017)	0.087(0.012)	0.656(0.043)	4.075(0.274)	6.546(0.114)	0.374(0.043)	0.071(0.010)	
62		0.078(0.011)	0.209(0.020)	0.974(0.056)	9.774(0.090)	2.221(0.001)	0.259(0.023)		
64		0.064(0.017)	0.371(0.031)	1.504(0.076)		1.071(0.026)	0.158(0.033)		
66	0.048(0.008)	0.102(0.014)	0.424(0.035)	2.947(0.137)	8.107(0.178)	0.497(0.036)			
68		0.138(0.020)	0.639(0.043)	7.684(0.225)	2.351(0.015)	0.316(0.024)	0.074(0.011)		
70	0.084(0.013)	0.195(0.022)	0.923(0.058)	1.741(0.083)	1.036(0.012)	0.178(0.015)			
72	0.042(0.007)	0.198(0.023)	1.542(0.082)	0.857(0.053)	0.565(0.050)	0.136(0.019)	0.053(0.008)	0.019(0.004)	
74	0.055(0.010)	0.278(0.027)	0.565(0.043)	0.419(0.035)	0.278(0.025)	0.084(0.012)			
76		0.297(0.045)		0.251(0.024)	0.247(0.018)	0.037(0.007)			
78		0.116(0.019)	0.172(0.019)	0.133(0.015)	0.073(0.012)				
80		0.072(0.013)	0.129(0.016)	0.097(0.013)	0.052(0.009)				
82		0.037(0.007)	0.070(0.037)		0.053(0.070)				
84			0.065(0.015)	0.030(0.010)					
86									
88			0.050(0.008)		0.022(0.005)				

[a] In units of 10^{-11}cm^3 s^{-1}. the error estimates, given in parentheses in the same units, include statistical errors accumulated during the analysis.

declines drastically as j_i increases; it is only 14% as large at $j_i = 76$ as it is at $j_i = 8$;

(2) Concurrently, the rotationally summed vibrationally inelastic rate constants for each value of Δv increase steadily with j_i and, consequently, so does the total vibrationally inelastic rate constant $k_{\Delta v}$. This increase, though fractionally more dramatic than the decrease in the rotationally inelastic rate constant, is not great enough to compensate for the falloff in the latter, with the result that

(3) The total inelastic rate constant k_{total} declines with increasing j_i. At $j_i = 76$, it is little more than half the $j_i = 8$ value.

C. Effect of Initial Vibration. Since our data were not taken at a constant v_i, it is important to know the effect of v_i on the inelastic rate constants. The recently reported results of Gao et al.[48] are of use here. They measured Li_2*−Ne inelastic rate constants for $j_i = 30$ and $2 \le v_i \le 24$. They found that the total vibrationally inelastic rate constant $k_{\Delta v}$ rose steadily with increasing v_i, while the rotationally inelastic rate constant declined slightly, with the result that the total inelastic rate constant was independent of v_i for $2 \le v_i \le 12$. The rise in $k_{\Delta v}$ was quite linear in this range and amounted to about 1.9×10^{-11}cm^3 s^{-1} per unit change of vibrational quantum number. Examination of the data for $j_i = 8$ and 22 in Table 7 makes it immediately clear that this rate of change must be strongly j_i-dependent. This observation is consistent with unpublished results[49] that indicate $k_{\Delta v} \approx 1 \times 10^{-11}$ cm^3 s^{-1} for $v_i = 0$, $j_i = 18$, more than an order of magnitude smaller than $k_{\Delta v} = 12.9 \times 10^{-11}$ cm^3 s^{-1} for $v_i = 9$, $j_i = 22$ from Table 7 and implying that the rate of rise of $k_{\Delta v}$ around $j_i = 20$ is about 1.9×10^{-11} cm^3 s^{-1} per unit change of vibrational quantum number. Consideration of these details does not alter the conclusions of section IIIB.

IV. Quasiclassical Trajectory Simulation of the Rate Constants

We have obtained rate constants from quasiclassical trajectory calculations for comparison with our data. Our classical trajectories program was developed by Smith[50] and is formulated using action-angle variables. The use of the canonically conjugate vibrational action v and vibrational phase Ψ_v offers two distinct advantages over methods using r (the internuclear separation) and p_r (its conjugate momentum). First, v and Ψ_v vary relatively slowly during the collision, eliminating the need for propagating the equations of motion with a time step small compared with the vibrational period. This is especially important when the atom and molecule are far apart. The result is that collisions at thermal velocities can be calculated rapidly

TABLE 6: Measured Inelastic Rate Constants for Li_2 $A^1\Sigma_u^+$−Ne Collisions with $j_i = 76$ and $v_i = 7$[a]

j_f	−4	−3	−2	−1	0	1	2	3	4
38						0.039(0.007)			
40									
42									
44									
46									
48							0.020(0.006)		
50						0.079(0.011)	0.075(0.010)		
52									
54						0.076(0.018)			0.050(0.010)
56							0.066(0.026)	0.082(0.022)	0.123(0.016)
58					0.051(0.007)		0.153(0.018)	0.146(0.019)	0.167(0.018)
60					0.081(0.021)	0.192(0.033)	0.181(0.020)	0.175(0.018)	
62				0.030(0.008)	0.104(0.013)	0.166(0.020)	0.338(0.080)	0.299(0.026)	0.311(0.026)
64					0.129(0.035)	0.242(0.026)	0.348(0.045)		0.509(0.037)
66		0.037(0.015)		0.079(0.011)		0.349(0.182)	0.509(0.034)	0.676(0.045)	
68		0.062(0.009)			0.297(0.026)	0.634(0.095)	0.535(0.040)	1.680(0.082)	0.375(0.030)
70		0.019(0.004)		0.104(0.015)	0.354(0.031)	1.157(0.061)	1.558(0.220)	0.331(0.061)	0.041(0.047)
72		0.052(0.028)	0.152(0.019)	0.183(0.019)	0.479(0.037)	2.035(0.039)	6.273(0.019)	0.656(0.044)	
74	0.045(0.009)		0.173(0.021)	0.216(0.054)	0.843(0.051)	5.342(0.049)	2.546(0.117)	0.262(0.024)	0.036(0.041)
76			0.150(0.022)	0.519(0.058)	1.735(0.083)		0.959(0.203)		
78			0.167(0.029)	0.789(0.039)	5.289(0.172)	4.693(0.137)	0.446(0.041)		
80	0.096(0.013)		0.280(0.028)	1.407(0.070)	6.417(0.206)	1.283(0.153)			
82	0.163(0.019)	0.139(0.022)	0.755(0.048)	1.506(0.189)	1.287(0.070)	0.514(0.037)			
84	0.123(0.015)	0.298(0.026)	0.203(0.024)	1.297(0.068)	0.534(0.038)	0.228(0.171)			
86	0.118(0.028)	0.195(0.026)		0.593(0.041)	0.174(0.020)	0.253(0.025)			
88	0.061(0.010)	0.140(0.016)		1.230(0.067)		0.031(0.006)			
90			0.133(0.019)	0.453(0.143)					

[a] In units of 10^{-11}cm^3 s^{-1}. The error estimates, given in parentheses in the same units, include statistical errors accumulated during the analysis.

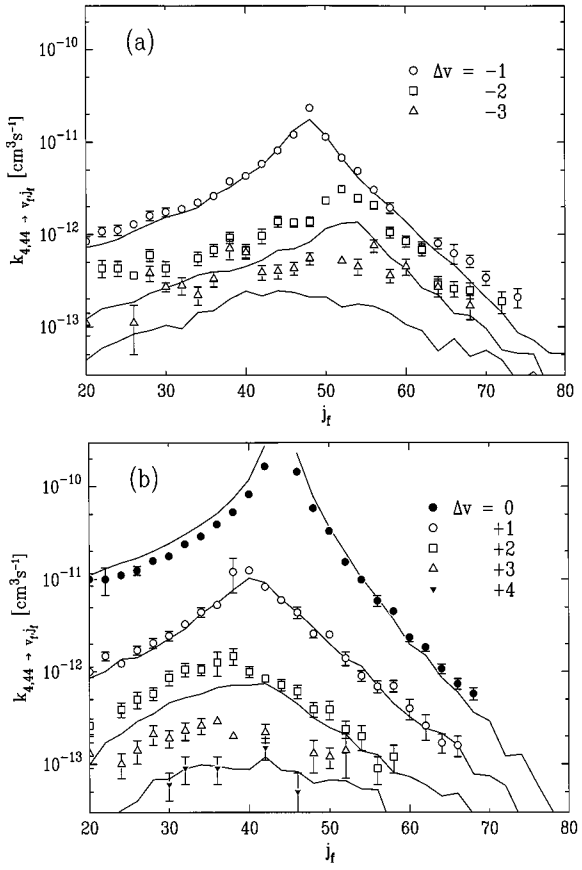

Figure 2. Inelastic Li_2*−Ne rate constant data for $j_i = 44$, $v_i = 4$. (a) Rate constants for $\Delta v < 0$; (b) rate constants for $\Delta v \geq 0$. Uncertainties were obtained as described in section II. The curves are rate constants from classical trajectories computed using an ab initio potential surface. For clarity, the computational results have been omitted for $\Delta v = +4$. There are no adjustable parameters in either the experiment or the computation.

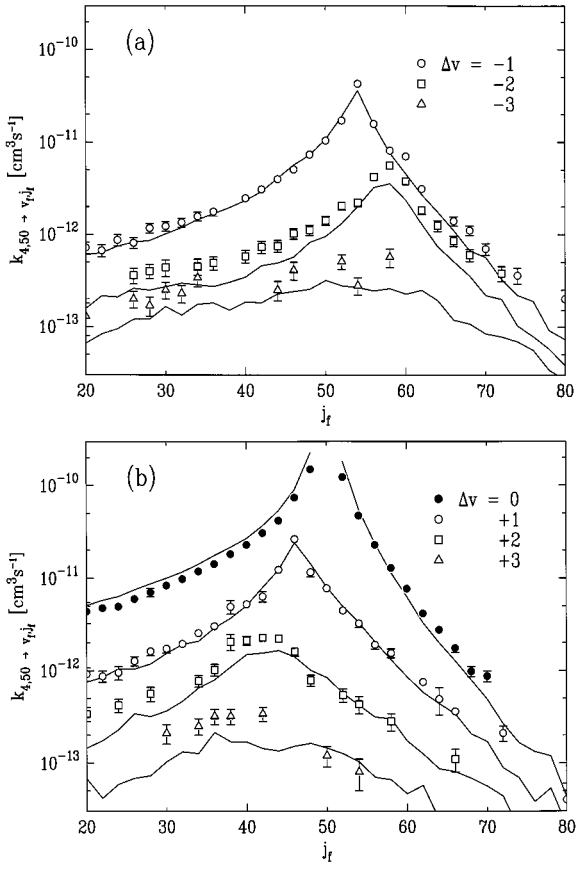

Figure 3. Inelastic Li_2*−Ne rate constant data for $j_i = 50$, $v_i = 4$. (a) Rate constants for $\Delta v < 0$; (b) rate constants for $\Delta v \geq 0$. Curves are from classical trajectories.

with modest computer equipment, and it is practical to explore the effect of a change in the initial values of the dynamical variables. The second advantage of action-angle variables lies in the accessibility of the classical analogue of the vibrational

TABLE 7: Rotationally Summed Inelastic Rate Constants in Units of 10^{-11}cm^3 s^{-1} [a]

		Δv									
j_i	v_i	−4	−3	−2	−1	0	+1	+2	+3	$k_{\Delta v}$	k_{total}
8	9				3.08(0.15)	130.5(5.7)				5.3(1.7)	134.7(6.5)
22	9			.57(0.13)	5.46(0.26)	104.1(3.1)				12.9(3.9)	117.0(5.0)
30	5			1.49(0.02)	6.24(0.04)	96.1(1.5)	3.77(0.05)	0.70(0.02)		13.4(0.2)	109.4(1.7)
44	4		.96(0.05)	2.59(0.09)	10.88(0.02)	78.8(1.8)	8.04(0.52)	1.34(0.07)	.32(0.03)	24.1(0.5)	103.0(1.9)
50	4		1.13(0.47)	3.54(0.17)	14.80(0.29)	65.1(1.2)	10.80(0.27)	2.07(0.10)	.32(0.04)	32.7(0.7)	97.8(1.3)
64	5		2.21(0.11)	6.79(0.19)	19.96(0.38)	36.4(0.6)	17.78(0.58)	5.55(0.66)	1.99(0.33)	54.3(1.0)	90.7(1.2)
76	7	1.52(0.26)	2.71(0.39)	8.94(0.49)	18.20(0.45)	18.2(0.5)	14.65(0.64)	5.19(0.46)	2.44(0.20)	54.6(1.2)	72.9(1.3)

[a] $k_{\Delta v} = 0$ is the rotationally inelastic rate constant, $k_{\Delta v}$ is the total vibrationally inelastic rate constant (excluding $\Delta v = 0$), and k_{total} is the total inelastic rate constant.

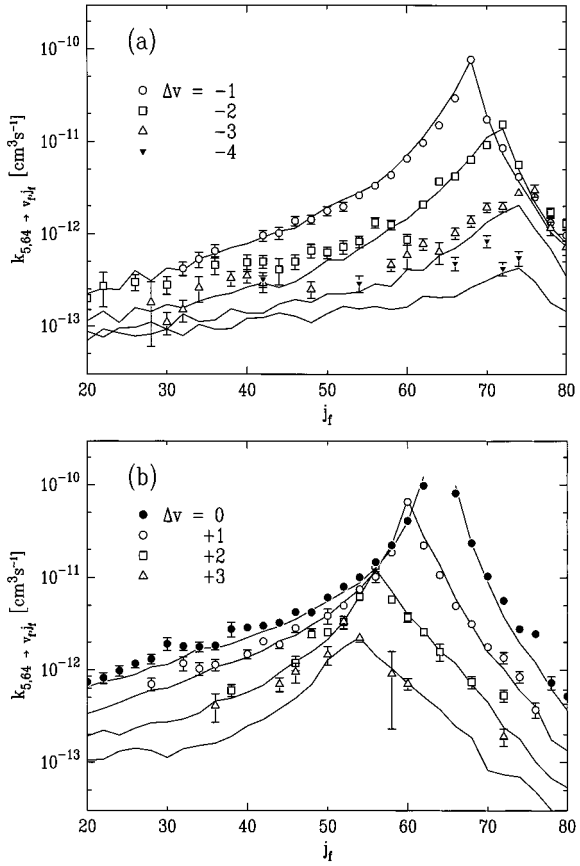

Figure 4. Inelastic Li_2*−Ne rate constant data for $j_i = 64$, $v_i = 5$. (a) Rate constants for $\Delta v < 0$; (b) rate constants for $\Delta v \geq 0$. Curves are from classical trajectories.

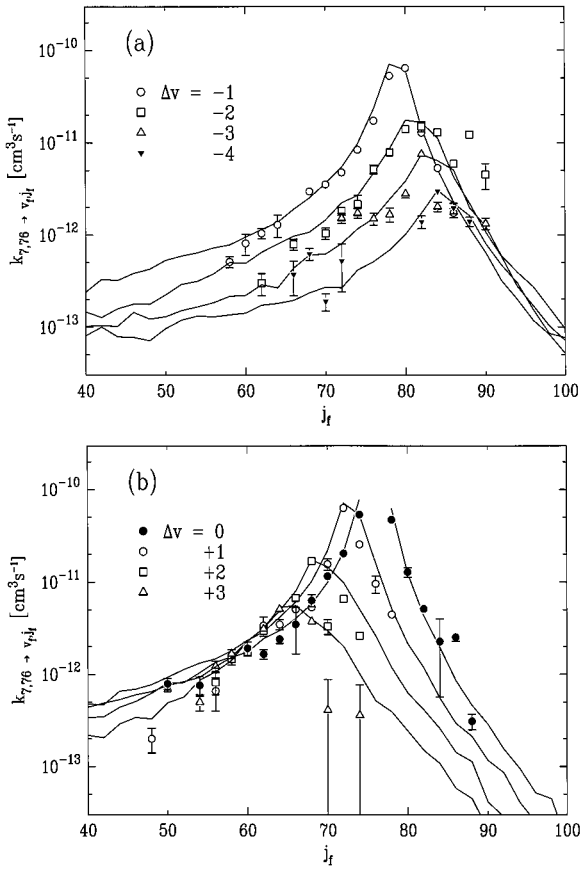

Figure 5. Inelastic Li_2*−Ne rate constant data for $j_i = 76$, $v_i = 7$. (a) Rate constants for $\Delta v < 0$; (b) rate constants for $\Delta v \geq 0$. Curves are from classical trajectories. Note the shift in the abscissa from previous figures.

quantum number at any time during the collision. Magill et al. have exploited this feature of the calculation to study the time evolution of v and j during individual collisions.[11,13]

Our calculations employed the ab initio potential surface computed for this system by Alexander and Werner.[51] The surface is one of the few that includes the variation of the internuclear separation r and hence is suitable for the computation of vibrationally inelastic trajectories. Alexander and Werner have used this potential in a close-coupled calculation of rotationally inelastic cross sections[51] and a coupled-states calculation of vibrotationally inelastic cross sections,[52] with generally good agreement with experimental results. The potential was calculated for only three internuclear separations and, strictly speaking, is valid only for $v \leq 3$; we have found, however, that in practice values of v_i as high as 7 may be reached without loss of the linear increase in the vibrationally inelastic cross section that is observed at lower v_i. Accordingly, we have carried out trajectory simulations of our data using the experimental value of v_i in each case. The range of validity of the potential with respect to the atom−molecule separation R is also limited, with the result that some trajectories must be discarded at the highest collision speeds. These speeds contribute little at the temperature of the experiment.

Trajectories were calculated for collision speeds ranging from 10 000 cm s^{-1} to 310 000 cm s^{-1} in increments of 20 000 cm s^{-1} for each value of j_i for which data were obtained. Additional velocities were added near the thresholds and peaks of the cross sections. A total of 200 000 trajectories were calculated for each velocity, resulting in an uncertainty in the largest calculated rate constants of less than 1%. The maximum impact parameter was chosen to give a converged determination of the cross sections.

Binning of the trajectories by the standard histogram method[53] was problematic. The coarse sieve of quantized bins into which classical outcomes are ordinarily sorted substantially broadened the narrow quasiresonant peaks, especially for $j_i = 64$, for which these features are particularly narrow (the j_f-distribution for $\Delta v = -1$ has a fwhm of only 2.9 $\hbar$). We circumvented this

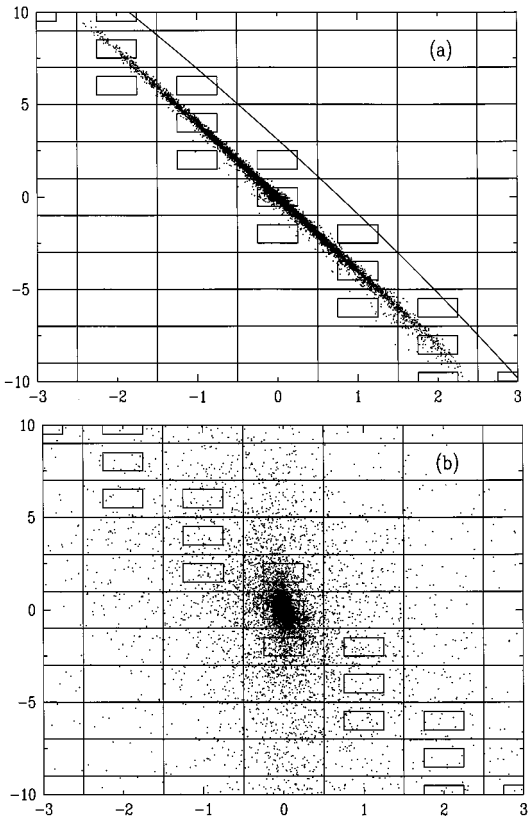

Figure 6. The final state of 4000 trajectories for $j_i = 64$ at collision speeds of (a) 70 000 cm s^{-1} and (b) 230 000 cm s^{-1}. Each dot represents one trajectory outcome and is plotted by the change in its rotational action Δj versus the change in its vibrational action Δv. The high degree of correlation of Δj and Δv at the lower collision speed is characteristic of quasiresonant (in this case resonant) vibrotational transfer. The boxes formed by the grid are the bins into which the continuously distributed results are quantized according to the standard histogram method. The smaller boxes are reduced in each dimension by a factor of 2. This reduction eliminates the "leakage" of trajectories into off-resonant bins that results in substantial broadening of the j_f distribution when the standard binning method is used. The region above the diagonal solid line in panel a is energetically inaccessible.

difficulty by reverting to the fully classical prescription for determining the cross sections, replacing the usual formula

$$\sigma(v_f, j_f) = \frac{\Delta\sigma}{\Delta v_f \Delta j_f} \tag{7}$$

by the continuous form

$$\sigma(v_f, j_f) = \frac{d^2\sigma}{dv_f\, dj_f} \tag{8}$$

We found in practice that simply reducing the vibrational bin width from 0.5 to 0.25 S was enough to mostly eliminate the broadening. Further reduction of the bin width continued to improve agreement with experiment in general, at the eventual cost of noisy cross sections due to the large number of omitted trajectories.

The origin of the broadening that standard binning produces, as well as the reason for the improvement in agreement resulting from reduced bin size, is shown in Figure 6. A single point is plotted to represent one trajectory outcome, resulting in what are essentially plots of trajectory density versus v_f and j_f. In Figure 6a, trajectories for a low collision speed are shown. They are grouped tightly along the energy resonant line of Eqn. 4. Superimposed is a grid of boxes representing the standard histogram binning procedure; the contents of each box are assigned to the value of v_f and j_f at the center of the box. The large size of the boxes in comparison with the width of the trajectory distribution results in many trajectories being assigned to nonresonant values of v_f and j_f — values not given by eq 4. The result is the broadening of the distribution previously noted. Reduction of the bin size, indicated by the smaller boxes superimposed upon the grid, eliminates these off-resonant contributions at this collision speed. The effect of reducing bin size is much smaller at higher collision speeds; Figure 6b shows that, since the trajectory outcomes are already distributed over an area large compared with the bin size, the effect on the density of bin size reduction is relatively small.

While a variety of alternative approaches to binning classical trajectories has been proposed over the years, particularly moment methods,[54,55] we feel that the adoption of the strictly classical definition of the cross section (eq 8) is most faithful to the classical mechanics, and we believe this approach merits study in greater detail as well as application in other classical simulations of resonant behavior.

As we found previously,[56] although the laser-excited collisional speed distribution can be reasonably well-represented by a Maxwellian distribution at a reduced "effective" temperature given by eq 3, it is more accurate to employ the correct laser-selected speed distribution.[56] Accordingly, we have numerically integrated cross sections obtained as described above using this distribution. The results of trajectory calculations binned in this fashion are shown with the experimental data in Figures 2−5. The agreement is essentially quantitative for small values of $|\Delta v|$.

Other workers have made quantum mechanical calculations that may be compared with our classical calculation. Maricq[57] used a potential previously employed by us before the ab initio potential became available, along with the coupled states approximation, to obtain cross section distributions for j_i ranging from 40 to 100 at a relative collision energy of 200 cm^{-1}, which corresponds to the effective mean thermal energy of our experiment. At $j_i = 64$, one final level dominates the distributions, just as in the experimental rate constant distributions. Alexander et al. have employed their vibrating ab initio potential and the coupled states approximation to generate cross section distributions for $j_i = 38-60$, again finding increasingly narrow distributions as j_i rises, with one final level dominant at the highest values of j_i. Unfortunately, it is currently impractical to carry out an exact close-coupled calculation for comparison with the classical calculation, because of the enormous number of magnetic sublevels that would be involved.

V. Discussion

The wide range of j_i spanned by our measured rate constants affords us the opportunity to study the onset of quasiresonance and its transformation into true energy resonance and to investigate the interplay of angular momentum and energy constraints. Parts a and b of Figure 7 show the Li_2* vibrotational levels in the vicinity of the initially populated level for $j_i = 64$ and 44. The largest measured rate constant for each v_f is indicated by a filled circle. At $j_i = 44$, energy resonance (i.e., intramolecular energy conservation) dictates that changes in v and j be correlated according to the rule $\Delta j = -6\Delta v$. Yet here, as at the higher j_i values studied, the observed rule is $\Delta j = -4\Delta v$. Here quasiresonance prevails: the j_f-distributions are sharply peaked, but shifted less than would be required to conserve intramolecular energy. At $j_i = 64$, however, the

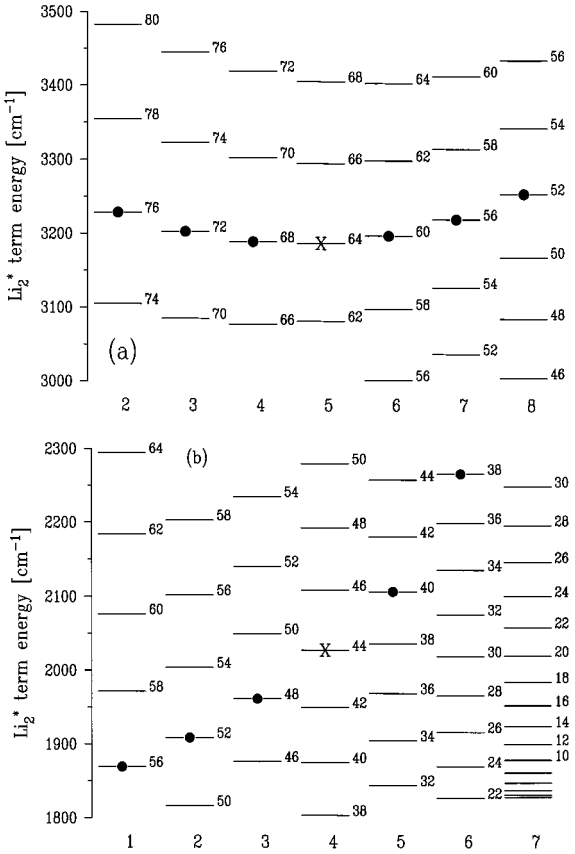

Figure 7. Li_2 A-state term energy level diagrams for (a) $j_i = 64$ and (b) $j_i = 44$, plotted versus vibrational quantum number. Each level is labeled by its j_f-value. The filled circles indicate the peak j_f for a given v_f. The initial level is marked by an X.

observed shift is truly energy resonant: the rotational energy level spacing at $j_i = 64$ is one-fourth the vibrational level spacing (see Figure 7a).

McKenzie has provided a semiclassical model based on first-order time-dependent perturbation theory that accounts qualitatively for these observations.[17,18] By factoring the transition matrix elements into time-dependent and time-independent parts, he was able to isolate two competing factors that together determine the most probable Δj for a given Δv. On one hand, the time-independent matrix elements sharply limit angular momentum transfer to small values. These matrix elements contain the geometric coupling of initial and transferred angular momenta. On the other hand, energy resonance in the time-dependent matrix elements, which contain the dynamics, strongly enhances the transition. Since the transition probability is proportional to the square of the product of these matrix elements, it will always be enhanced by energy resonance but can only be large if the initial and final levels have nearly the same value of j. In H_2–He, the time-independent matrix elements for $\Delta j = 0$, 2, 4, and 6 are in the ratio 0.2:0.1:0.01:0.0002. The steep falloff for $\Delta j > 2$ makes quite plausible the observed rule $\Delta j^{peak} = -2\Delta v$ for this system. Values of Δv greater than 1 can be accommodated if one assumes that they proceed via coupling through a sequence of intermediate states given by the above rule. In the present case of Li_2*−Ne, resonance is observed at $j_i = 64$. The fact that the peak shift does not increase at smaller j_i is consistent with McKenzie's results.

We are now in a position to understand why only molecules with small moments of inertia such as H_2, Li_2, and hydrides exhibit vibration−rotation resonance. Coincidence or near-coincidence in energy of rotational levels for different v is not a sufficient condition; the levels must in addition differ by only a few units of angular momentum. This will occur at moderate j only in molecules with a small moment of inertia, and hence, a relatively large rotational constant B_e compared with ω_e. As McKenzie emphasized, it is the ratio B_e/ω_e that determines the onset of resonance, although the rate of approach to resonance may be difficult to predict a priori. McCaffery[8,58] has recently developed a graphical approach that may give insight into the approach to resonance and help to define the quasiresonant regime. By plotting the collisional energy and orbital angular momentum in the $\Delta j - v_{rel}$ plane, he has provided an intuitively appealing way of seeing the interplay of energy and angular momentum for different values of j_i.

TABLE 8: Vibrational and Rotational Frequencies of Li_2 $A^1\Sigma_u^+$ in Units of 10^{12} rad/s^{-1}

j_i	v_i	ω_v	ω_j	ω_v/ω_j
8	9	42.52	1.43	29.78
22	9	42.10	3.73	11.29
30	5	43.98	5.23	8.42
44	4	43.53	7.48	5.82
50	4	42.99	8.34	5.16
64	5	40.91	10.04	4.08
76	7	38.24	11.07	3.46

A detailed analysis of a classical trajectory calculation similar to that reported in section IV has resulted in a great deal of insight into the classical mechanism of quasiresonant V−R transfer.[7,11,13] We provide here a brief synopsis of the interpretation that has emerged and refer the reader to our other publications for greater detail. In the classical point of view, it is the frequencies of vibration and rotation, and their relationship to the collision duration, that determine the onset of quasiresonant transfer. The relevant molecular frequencies for Li_2*, calculated from the Dunham coefficients,[38] are given in Table 8. Entries for $j_i = 8$, 22, and 30 are included so that the data of refs 12 and 48 may be compared with the present results.

At low j_i and thermal collision speeds, many complete vibrations occur during the time of significant atom−diatom interaction, with the force on the oscillator peaking near the vibrational outer turning point. Such collisions tend to be vibrationally adiabatic; the atom−molecule force is nearly symmetric about the vibrational outer turning point because the relative atom−diatom position changes little during a vibrational period. The force is averaged away, and the net vibrational impulse is very small. This is the well-known state of affairs that produces vibrationally inelastic cross sections that are generally small compared with rotationally inelastic cross sections at thermal velocities for reasonably tightly bound molecules. In the high j_i regime, however, rotation determines the form of the time dependent force. When several rotations occur during the collision, the molecular anisotropy leads to a modulation of the time-dependent interaction potential at the effective rotational frequency rather than the vibrational frequency, and the forcing function breaks up into a sequence of sharp maxima due to the exponential nature of the interaction.[7] These subcollisions enhance vibrational transfer in just the way first envisioned by Cottrell and Matheson. Moreover, at a resonance such as $j_i = 64$ in Li_2*, the inelasticities produced by successive subcollisions reinforce one another and produce the negative correlation between Δv and Δj in the manner we have described previously.[7] The transition between dynamical regimes is controlled by the vibrational and rotational frequencies, the collision speed, and the steepness of the repulsive potential.

The effective frequency at which the rotation modulates the atom−molecule force during the collision is twice the angular

frequency of the molecule owing to the homonuclear symmetry of Li_2. At $64 > j_i > 42$, quasiresonance prevails; at $j_i = 64$, this effective rotational frequency is half the vibrational frequency. At the yet higher $j_i = 130$, a 1:1 resonance is expected;[11] in fact, for $v_i = 3$ and $j_i = 130$, the ratio of vibrational to effective rotational frequencies is 1.0005, and the reduced angular momentum transfer required should allow energy resonance to result in even larger vibrotationally inelastic cross sections than those observed at $j_i = 64$. Stwalley and co-workers[59] have proposed a scheme for "spinning up" molecules to such extreme angular momentum levels, holding out the possibility of experimentally observing the 1:1 resonance.

The observation that the single ratio $\Delta j/\Delta v = -4$ persists away from energy resonance in both the experiments and classical trajectory calculations has led us to propose that a frequency locking mechanism is operative in this system.[11] This has been confirmed by the analysis of Hoving and Parson,[60] who used the theory of adiabatic invariants to show that the phase space for this system is partitioned into isolated resonance zones. These resonance zones extend over a range of j, giving rise to the "plateaus" with fixed $\Delta j/\Delta v$ ratios that we observed both experimentally and in trajectory calculations.[11] However, their analysis does not predict the extent and onset of quasiresonance.

With the production of ultracold molecules becoming a reality,[61,62] the question arises as to the limits of the resonant rise of the cross section with diminishing collision speed. Forrey et al.[9] have explored quasiresonance at very low collision speeds using quasiclassical trajectories and found the strong correlation of Δv and Δj to persist in plots such as Figure 6a. However, the final state density did not extend beyond the elastic bin. Lacking a means for extrapolating the final state density into the inelastic bins, they were unable to estimate the inelastic cross sections. We have found, for collisions at the highly resonant $j_i = 64$ calculated classically on the Alexander−Werner potential surface, that vibrationally inelastic transfer with substantial binned cross section can occur down to a extremely low collision speeds.[63] We are studying this behavior with the intention of making concrete suggestions for experimental work.

Acknowledgment. The experimental component of this work was supported by National Science Foundation Grant No. CHE-8421392. Acknowledgment is made to the donors of the Petroleum Research Fund, administered by the American Chemical Society, for the support of this research.

References and Notes

(1) Yardley, J. T. *Introduction to Molecular Energy Transfer*; Academic Press: New York, 1980.
(2) Cottrell, T. L.; Matheson, A. J. *Proc. Chem. Soc.* **1962**, *1962*, 17.
(3) Cottrell, T. L.; Matheson, A. J. *Trans. Faraday Soc.* **1962**, *58*, 2336.
(4) Saenger, K. L.; Smith, N.; Dexheimer, S. L.; Engelke, C.; Pritchard, D. E. *J. Chem. Phys.* **1983**, *79*, 4076.
(5) Scott, T. P. Ph.D. Thesis, M. I. T.: Cambridge, Massachusetts, 1985 (unpublished).
(6) Scott, T. P.; Smith, N.; Magill, P. D.; Pritchard, D. E.; Stewart, B. *J. Phys. Chem.* **1996**, *100*, 7981.
(7) Stewart, B.; Magill, P. D.; Scott, T. P.; Derouard, J.; Pritchard, D. E. *Phys. Rev. Lett.* **1988**, *60*, 282.
(8) McCaffery, A. J. *J. Chem. Phys.* **1989**, *111*, 7697.
(9) Forrey, R. C.; Balakrishnan, N.; Dalgarno, A.; Haggerty, M. R.; Heller, E. J. *Phys. Rev. Lett.* **1999**, *82*, 2657.
(10) Balakrishnan, N.; Vieira, M.; Babb, J. F.; Dalgarno, A.; Forrey, R. C.; Lepp, S. *Astrophys. J.* **1999**, *524*, 1122.
(11) Magill, P. D.; Stewart, B.; Smith, N.; Pritchard, D. E. *Phys. Rev. Lett.* **1988**, *60*, 1943.
(12) Magill, P. D.; Scott, T. P.; Smith, N.; Pritchard, D. E. *J. Chem. Phys.* **1989**, *90*, 7195.
(13) Magill, P. D. Ph.D. Thesis, M. I. T.: Cambridge, Massachusetts, 1987 (unpublished).
(14) Dexheimer, S. L.; Brunner, T. A.; Pritchard, D. E. *J. Chem. Phys.* **1983**, *79*, 5206.
(15) Rabitz, H.; Zarur, G. *J. Chem. Phys.* **1974**, *61*, 5076.
(16) Alexander, M. H. *J. Chem. Phys.* **1974**, *61*, 5167.
(17) McKenzie, R. L. Ph.D. Thesis, NASA Technical Report TR-R-466, National Aeronautics and Space Administration, Washington, DC, 1976.
(18) McKenzie, R. L. *J. Chem. Phys.* **1977**, *66*, 1457.
(19) Alexander, M. H. *J. Chem. Phys.* **1977**, *66*, 4608.
(20) Dove, J. E.; Raynor, S.; Teitelbaum, H. *Chem. Phys.* **1980**, *50*, 175.
(21) Thompson, D. L. *J. Chem. Phys.* **1981**, *75*, 1829.
(22) Flower, D. R.; Kirkpatrick, D. J. *J. Phys. B* **1982**, *15*, L11.
(23) Blais, N. C.; Truhlar, D. G. *J. Chem. Phys.* **1978**, *69*, 846.
(24) Blais, N. C.; Truhlar, D. G. *J. Phys. Chem.* **1982**, *86*, 638.
(25) Thompson, D. L. *J. Chem. Phys.* **1983**, *78*, 1763.
(26) Thompson, D. L. *J. Chem. Phys.* **1982**, *76*, 5947.
(27) Thompson, D. L. *J. Phys. Chem.* **1982**, *86*, 630.
(28) At $j_i = 34$ the molecular term energy lies several electron volts above the dissociation limit!
(29) Kurzel, R. B.; Steinfeld, J. I.; Hatzenbuhler, D. A.; Leroi, G. E. *J. Chem. Phys.* **1971**, *55*, 4822.
(30) Ennen, G.; Ottinger, Ch. *Chem. Phys.* **1974**, *3*, 404.
(31) Zittel, P. F.; Moore, C. B. *J. Chem. Phys.* **1973**, *58*, 2004
(32) Perrin, M. Y.; Jolicard, G. *Chem. Phys. Lett.* **1986**, *127*, 1986.
(33) Moore, C. B. *J. Chem. Phys.* **1965**, *43*, 2979.
(34) Cottrell, T. L.; Dobbie, R. C.; McLain, J.; Read, A. W. *Trans. Faraday Soc.* **1964**, 9.
(35) Walkup, R.; Spielfiedel, A.; Ely, D.; Phillips, W. D.; Pritchard, D. E. *J. Phys. B.* **1981**, *14*, 1953.
(36) Smith, N. Ph.D. Thesis; M. I. T.: Cambridge, Massachusetts, 1983 (unpublished).
(37) Stewart, B. Ph.D. Thesis; M. I. T.: Cambridge, Massachusetts, 1987 (unpublished).
(38) Kusch, P.; Hessel, M. M. *J. Chem. Phys.* **1977**, *67*, 586.
(39) Verma, K. K.; Koch, M. E.; Stwalley, W. C. *J. Chem. Phys.* **1983**, *78*, 3614.
(40) Barakat, B.; Bacis, R.; Carrot, F.; Churassy, S.; Crozet, P.; Verges, J. *Chem. Phys.* **1986**, *102*, 215.
(41) Schmidt-Mink, I.; Müller, W.; Meyer, W. *Chem. Phys.* **1985**, *92*, 263.
(42) Baumgartner, C.; Kornmeier, H.; Preuss, W. *Chem. Phys. Lett.* **1984**, *107*, 13.
(43) Preuss, W.; Baumgartner, G. *Z. Phys. A* **1985**, *320*, 125.
(44) Derouard, J.; Sadeghi, N. *Chem. Phys.* **1984**, *88*, 171.
(45) Nesmeyanov, A. N. *Vapor Pressure of the Chemical Elements*; Gary, R., Ed.; Elsevier: Amsterdam, 1963.
(46) Baumgartner, G.; Keller, H. P.; Preuss, W. *Z. Phys. D* **1986**, *1*, 295.
(47) Scott, T. P.; Smith, N.; Pritchard, D. E. *J. Chem. Phys.* **1984**, *80*, 4841.
(48) Gao, Y.; Gorgone, P. S.; Davis, S.; McCall, E. K.; Stewart, B. *J. Phys. Chem.* **1994**, *104*, 1415.
(49) Stewart, B. Unpublished results.
(50) Smith, N. *J. Chem. Phys.* **1986**, *85*, 1987.
(51) Alexander, M. H.; Werner, H. J. *J. Chem. Phys.* **1991**, *95*, 6524.
(52) Alexander, M. H.; Berning, A.; Degli Esposti, A.; Joerg, A.; Kliesch; Werner, H.-J. *Ber. Bunsen-Ges. Phys. Chem.* **1990**, *94*, 1253.
(53) Pattengill, M. D. In *Atom-Molecule Collision Theory: A Guide for the Experimentalist*; Bernstein, R. B., Ed.; Plenum: New York, 1979.
(54) Bowman, J.; Leasure, S. C. *J. Chem. Phys.* **1977**, *66*, 1756.
(55) Truhlar, D. G.; Reid, B. P.; Zurawski, D. E.; Gray, J. C. *J. Phys. Chem.* **1981**, *85*, 786.
(56) Gao, Y.; Stewart, B. *J. Chem. Phys.* **1995**, *103*, 860
(57) Mariq, M. *Phys. Rev. A* **1989**, *39*, 3710.
(58) McCaffery, A. J. *J. Phys. Chem. A* **2000**, *104*, 10440.
(59) Jing, Li; Bahns, J. T.; Stwalley, W. C. *J. Chem. Phys.* **2000**, *112*, 6255.
(60) Hoving, W. J.; Parson, R. *Chem. Phys. Lett.* **1989**, *158*, 222.
(61) Nikolov, A. N.; Ensher, J. R.; Eyler, E. E.; Wang, H.; Stwalley, W. C.; Gould, P. L. *Phys. Rev. Lett.* **2000**, *84*, 246.
(62) Wynar, R.; Freeland, R. S.; Han, D. J.; Ryu, C.; Heinzen, D. J. *Science* **2000**, *287*, 1016.
(63) Stewart, B. In preparation.